# Variable-charge interatomic potentials for molecular-dynamics simulations of TiO$_2$

Shuji Ogata[a]
*Department of Applied Sciences, Yamaguchi University, Ube 755-8611, Japan*

Hiroshi Iyetomi
*Department of Physics, Niigata University, Niigata 950-2181, Japan*

Kenji Tsuruta
*Department of Electrical and Electronic Engineering, Okayama University, Okayama 700-8530, Japan*

Fuyuki Shimojo
*Faculty of Integrated Arts and Sciences, Hiroshima University, Higashi-Hiroshima 739-8521, Japan*

Rajiv K. Kalia, Aiichiro Nakano, and Priya Vashishta
*Concurrent Computing Laboratory for Materials Simulation, Department of Physics and Astronomy and Department of Computer Science, Louisiana State University, Baton Rouge, Louisiana 70803-4001*

An interatomic potential model has been developed for molecular-dynamics simulations of TiO$_2$ (rutile) based on the formalism of Streitz and Mintmire [J. Adhes. Sci. Technol. **8**, 853 (1994)], in which atomic charges vary dynamically according to the generalized electronegativity equalization principle. The present model potential reproduces the vibrational density of states, the pressure-dependent static dielectric constants, the melting temperature, and the surface relaxation of the rutile crystal, as well as the cohesive energy, the lattice constants, and the elastic moduli. We find the physical properties of rutile are significantly affected by dynamic charge transfer between Ti and O atoms. The potential allows us to perform atomistic simulations on nanostructured TiO$_2$ with various kinds of interfaces (surfaces, grain boundaries, dislocations, etc.). © *1999 American Institute of Physics.* [S0021-8979(99)07618-5]

## I. INTRODUCTION

Titanium dioxide is an important ceramic for a variety of current and future industrial applications: ultralarge scale integration (ULSI) chips,[1] oxygen-gas sensors,[2] and purification of nanopowders[2] using photocatalysis-assisted molecular disintegration, etc.[3] These applications stem from high polarizability and large static dielectric constant[4] ($\sim$114 for powdered rutile structure), as well as high rates of oxidation and reduction reactions of TiO$_2$ surfaces and interfaces.[2] In the vicinity of interfaces TiO$_2$ exhibits significant charge fluctuations, which is evident from the nonstoichiometric Ti$_x$O$_{2x-1}$ (with $x$ ranging from 4 to 10) in interfacial regions.

Molecular dynamics (MDs) simulations of TiO$_2$ systems are particularly challenging because of the sensitivity of the charge transfer among Ti and O atoms to the local environment. Several attempts have been made to carry out atomistic simulations of TiO$_2$. None of them take into account variations in atomic charges caused by changes in the local environment around atoms.[5-7] Catlow *et al.*[5] have developed a shell-model interatomic potential for the rutile crystal structure of TiO$_2$. In this model the valence electrons of each atom form a spherical shell of a fixed radius which is connected to the atomic core by a ''spring.'' Results for elastic moduli and dielectric constant of rutile in the shell model are in good agreement with experiments. Direct application of

the shell model to surface or interface systems is, however, difficult since the model does not take into account variations in charge transfer among the atoms.

Recently Streitz and Mintmire[8] proposed a variable-charge interatomic potential for bulk rutile TiO$_2$. This potential allows atomic charges to vary dynamically in response to changes in the local environment; charges are determined by setting generalized electronegativities of all the atoms equal to one another. The calculated lattice constant, cohesive energy, and elastic moduli are in reasonable agreement with experimental results. However, results for the dielectric constant ($\epsilon_{xx}=3.5$ and $\epsilon_{zz}=3.0$) are an order of magnitude lower than the experimental values (see Table II).

We have modified the interaction potential of Streitz and Mintmire so that it can correctly describe the dielectric properties while maintaining the good agreement between the calculated and experimental values of the lattice constant, cohesive energy, and elastic moduli of the rutile TiO$_2$. Our results for the phonon density-of-states (DOS) and the pressure dependence of $\epsilon_{xx}$ and $\epsilon_{zz}$ agree well with experimental measurements. Through detailed analyses of the calculated electric-dipole oscillations, we elucidate the characteristic features of the Ti–O bonding that play an important role in reproducing the macroscopic and microscopic quantities with accuracy comparable to those of first-principles calculations.

---

[a]Electronic mail: ogata@po.cc.yamaguchi-u.ac.jp

J. Appl. Phys., Vol. 86, No. 6, 15 September 1999

Ogata *et al.*    3037

## II. FORMULATION

Let us consider a charge-neutral system composed of $N_{\text{Ti}}$ titanium and $N_{\text{O}}$ ($=2N_{\text{Ti}}$ for TiO$_2$) oxygen atoms with masses $\{m_i\}$ and charges $\{q_i e\}$ located at $\{\vec{R}_i\}$ ($i = 1,2,...,N_{\text{Ti}}+N_{\text{O}}$). The Hamiltonian of the system is $H = \Sigma_i m_i |\dot{\vec{R}}_i|^2/2 + E_{\text{tot}}$, where the total potential energy, $E_{\text{tot}}$, is taken to be a sum of four terms

$$E_{\text{tot}} = \sum_i E_i^{\text{atom}}(q_i) + \sum_{i<j} V_{ij}^{\text{es}}(R_{ij};q_i,q_j) + \sum_{i<j} V_{ij}^c(R_{ij})$$

$$+ \sum_{i \in (\text{Ti}), j \in (\text{O})} \Delta V_{ij}^{\text{TiO}}(R_{ij};q_i,q_j). \qquad (1)$$

The first term in the righthand side of Eq. (1) represents the atomic energy, which is expanded in terms of $q_i$ to second order as

$$E_i^{\text{atom}}(q_i) = E_i^{\text{atom}}(O) + q_i \chi_i + \tfrac{1}{2} J_i q_i^2. \qquad (2)$$

Here $\chi_i$ and $J_i$ are referred to as the electronegativity and hardness, respectively.[8–11] They are taken to be free parameters that are determined by optimizing the potential energy. The second term in Eq. (1) denotes the electrostatic interaction energy[8,10]

$$V_{ij}^{\text{es}}(R_{ij};q_i,q_j) = \int d\vec{r}_1 \int d\vec{r}_2 \frac{\rho_i(\vec{r}_1,q_i)\rho_j(\vec{r}_2,q_j)}{r_{12}}, \qquad (3)$$

where

$$\rho_i(\vec{r},q_i) = Z_i e \delta(|\vec{r}-\vec{R}_i|) + (q_i e - Z_i e) f_i(|\vec{r}-\vec{R}_i|) \qquad (4)$$

is the charge-density distribution around the $i$-th atom with a ''core'' charge $Z_i e$ and a normalized valence-electron density distribution $f_i$. As in the original parameterization[8] we take $Z_{\text{Ti}}=4$, $Z_{\text{O}}=0$, and $f_i$ to be a $1s$-like function

$$f_i(r) = (\zeta_i^3/\pi)\exp(-2\zeta_i r). \qquad (5)$$

The third term in Eq. (1) primarily represents the covalent bonding resulting from hybridization of valence electrons and the steric repulsion between the atomic cores. Following Streitz and Mintmire,[8,10] we adopt a modified Rydberg form for $V_{ij}^c$

$$V_{ij}^c(R_{ij}) = -C_{ij}[1+(R_{ij}-R_{ij}^e)/l_{ij}]\exp[-\alpha_{ij}(R_{ij}-R_{ij}^e)/l_{ij}]. \qquad (6)$$

After substituting Eq. (4) in Eq. (3), we follow Streitz and Mintmire and omit terms proportional to $Z_i Z_j$,[10] since they are independent of both $q_i$ and $q_j$ and hence may be regarded as effectively included in $V_{ij}^c$. First-principles calculations[12] have shown that atoms in the vicinity of surfaces move away substantially from the crystalline sites. The Rydberg-like form, Eq. (6), is too restrictive to take account of this behavior. The last term in Eq. (1), involving only neighboring Ti and O atoms, is introduced to include the surface relaxation effects when the smallest surface-energy plane [i.e., (110)] is created. We take it to be of the form

$$\Delta V_{ij}^{\text{TiO}}(R_{ij},q_i,q_j) = \tau[q_{\text{o}}+q_{\text{Ti}}g(R_{ij})]^2 h(R_{ij}), \qquad (7)$$

with

$$h(R) = \frac{1+\exp[(\xi-R)/\sigma]}{1+\exp[(R-\gamma)/\eta]} \qquad (8)$$

and

$$g(R) = 1.5 - \frac{1}{1+\exp[(\lambda-R)/w]}. \qquad (9)$$

In Eq. (8) the neighboring Ti–O pairs with distances, $R$, less than $\sim\gamma$ are used in the denominator on the righthand side. The numerator of $h(R)$, on the other hand, controls the anharmonic vibrations between Ti–O pairs. Therefore, we choose its functional parameters to adjust the melting temperature of the rutile structure. The effect of $g(R)$ in $\Delta V_{ij}^{\text{TiO}}$ on charge transfer between Ti and O atoms will be discussed in Sec. IV.

The electrostatic potential, $V_{ij}^{\text{es}}$, is decomposed into the Coulomb term $q_i q_j e^2/R_{ij}$ and the residual short-range term $V_{\text{SR},ij}^{\text{es}} \equiv V_{ij}^{\text{es}} - q_i q_j e^2/R_{ij}$. The Coulomb interaction is calculated using the Ewald method[13] and the short-range term is truncated at a cutoff distance $R_c$.

$$\tilde{V}_{\text{SR},ij}^{\text{es}}(R) \equiv \begin{cases} V_{\text{SR},ij}^{\text{es}}(R) - V_{\text{SR},ij}^{\text{es}}(R_c) - (R-R_c)[dV_{\text{SR},ij}^{\text{es}}(R)/dR]_{R=R_c} & \text{for } R \leqslant R_c \\ 0 & \text{for } R > R_c \end{cases}. \qquad (10)$$

Note the potential, $\tilde{V}_{\text{SR},ij}^{\text{es}}$, and the corresponding force are continuous at $R_c$. The short-range covalent bonding term, $V_{ij}^c$, in Eq. (3) is also truncated in the same way as $V_{\text{SR},ij}^{\text{es}}$ with the same cutoff distance.

The parameters $\{\chi_i, J_i, \zeta_i, C_{ij}, R_{ij}^e, l_{ij}, \alpha_{ij}, \lambda, w, \gamma, \tau, \eta, \xi, \sigma\}$ in the potential are determined by fitting to experimental and first-principles electronic structure calculations of the lattice constant, cohesive energy, elastic moduli, static dielectric constants, surface energies of low-index planes [(110) and (100)], melting temperature at ambient pressures, and surface relaxation properties for (110) of the rutile struc-ture. Atomic charges, $q_i$, are determined dynamically in MD simulations by minimizing $E_{\text{tot}}$ with respect to a set $\{q_i\}$ under the constraint of charge conservation. Table I lists values of the parameters so determined with $R_c=9$ Å. The melting temperature in Table II is calculated with the constant-$NPT$ MD simulation using $N_{\text{Ti}}+N_{\text{O}}=1050$. Our values for the electronegativity $\chi_O=5.44$ eV and the hardness $J_O=8.25$ eV for oxygen compare well with $\chi_O=8.7$ eV and $J_O=13.4$ eV evaluated by Rappe and Goddard[11] using the atomic data. The reliability of the present interaction scheme will be demonstrated in Sec. III.

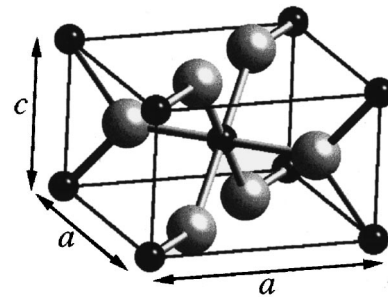TABLE I. Optimized values of the potential parameters in the present model.

| | Parameters in Eqs. (2), (4), and (5). | | | |
| | $\chi_i$ (eV) | $J_i$ (eV) | $\zeta_i$ (Å$^{-1}$) | $Z_i$ |
|---|---|---|---|---|
| Ti | 0 | 10.3 | 0.530 | 4.0 |
| O | 5.44 | 8.25 | 0.720 | 0.0 |

| | Parameters in Eq. (6) | | | |
| | $R_{ij}^e$ (Å) | $l_{ij}$ (Å) | $C_{ij}$ (eV) | $\alpha_{ij}$ |
|---|---|---|---|---|
| Ti–Ti | 2.85 | 0.130 | 0.281 | 1.0 |
| Ti–O | 2.53 | 0.504 | 0.104 | 1.0 |
| O–O | 3.47 | 0.490 | 0.0704 | 1.27 |

| | Parameters in Eqs. (7)–(9) | | | | | |
| | $\lambda$ (Å) | $w$ (Å) | $\tau$ (eV) | $\gamma$ (Å) | $\eta$ (Å) | $\xi$ (Å) | $\sigma$ (Å) |
|---|---|---|---|---|---|---|---|
| Ti–O | 1.76 | 0.018 | 16.33 | 2.50 | 0.30 | 0.60 | 0.20 |



FIG. 1. Rutile structure of TiO$_2$. Small and large spheres represent Ti and O atoms, respectively.

## III. COMPARISON OF VARIOUS QUANTITIES WITH EXPERIMENTAL DATA

The rutile (tetragonal) structure of TiO$_2$ is depicted in Fig. 1: Ti atoms (smaller spheres) are located at $(x,y,z)$ $=(0,0,0)$ and $(1/2, 1/2, 1/2)$ in scaled coordinates; O atoms (larger spheres) are at $(u,u,0)$, $(1-u,1-u,0)$, $(1/2-u,1/2+u,1/2)$, and $(1/2+u,1/2-u,1/2)$. The calculated results for the lattice constants $a$, $c$, and $u$ at aero pressure agree well with the experimental values,[14] see Table II. In bulk rutile the equilibrium atomic charge number for Ti is $q_{Ti}=2.43$, which compares favorably with the value (2.6) obtained by fitting experimental phonon-dispersion relations.[15] In the tight-binding calculation[16] for bulk rutile, $q_{Ti}=2.36$ and $q_O =-1.18$. The calculated cohesive energy, $E_c \equiv -E_{tot} + \Sigma_i E_i^{atom}(0)$, of TiO$_2$ in the rutile structure also agrees very well with the experimental value,[17] see Table II. Results for elastic moduli are also given in Table II.[18] Their accuracy is

comparable to that of those calculated with the Streitz–Mintmire potentials (see Table III in Ref. 8). If the atomic charges are taken to be the bulk equilibrium values, the elastic moduli are approximately 10% larger than the present values.

Partial and total phonon (DOS) of TiO$_2$ in the rutile structure are calculated from the dynamical matrix and also from Fourier transforms of velocity-autocorrelation functions. As shown in Fig. 2, the results with the two approaches are in excellent agreement with each other. In Fig. 2 we also compare our results with experimental data[15] [Fig. 2(c)] and with the results based on the Streitz–Mintmire

TABLE II. Comparison of the theoretical results based on the present potential model with experimental data for various quantities of bulk rutile.

| | Theory | Experiment |
|---|---|---|
| $a$ (Å) | 4.6781 | 4.5936[a] |
| $c$ (Å) | 2.5818 | 2.5987[a] |
| $u$ | 0.2971 | 0.3048[a] |
| $q_{Ti}$ | 2.43 | 2.6[b] |
| $E_c/N_{Ti}$ (eV) | 19.8 | 19.8[c] |
| bulk modulus (GPa) | 228 | 216[d] |
| $C_{11}$ (GPa) | 412 | 271[d] |
| $C_{33}$ (GPa) | 519 | 484[d] |
| $C_{44}$ (GPa) | 136 | 124[d] |
| $C_{66}$ (GPa) | 119 | 195[d] |
| $C_{12}$ (GPa) | 107 | 178[d] |
| $C_{13}$ (GPa) | 123 | 150[d] |
| $\epsilon_{xx}$ | 91.8 | 86[e] |
| $\epsilon_{zz}$ | 195.9 | 170[e] |
| melting temperature (K) | 2000–2400 | 2100[f] |

[a]Reference 14.
[b]Reference 15.
[c]Reference 17.
[d]Reference 18.
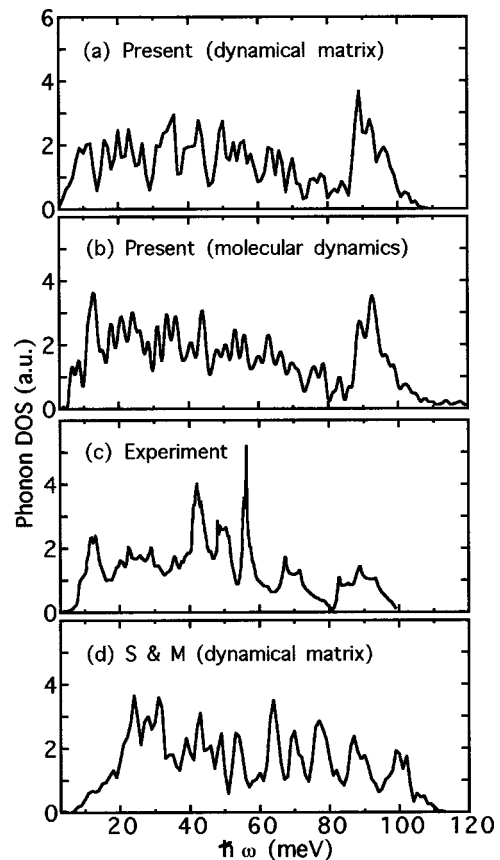[e]Reference 20.
[f]Reference 4.



FIG. 2. Phonon densities-of-states of rutile: (a) calculated by diagonalizing the dynamical matrix with the present potential, (b) obtained from MD simulation performed at 100 K using the present potential, (c) result of a neutron-scattering experiment (see Ref. 15), (d) calculated by diagonalizing the dynamical matrix with the Streitz–Mintmire potential (Ref. 8).

potential[8] [Fig. 2(d)]. The calculated peak positions and their relative intensities, including the peak structure below 20 meV and the pseudogap around 80 meV, are consistent with experimental results. The features below 20 meV and the pseudogap around 80 meV are not present in the results calculated with the Streitz–Mintmire potential. In the theoretical calculations for DOS, we took a system consisting of $N_{Ti} + N_O = 672$ atoms under the periodic boundary conditions. We then executed the MD simulations at $T = 100$ K to calculate the velocity-autocorrelation functions or diagonalized the dynamical matrix for the ground state at $T = 0$ K to obtain the phonon modes.

Static dielectric constants of $TiO_2$ in the rutile structure are determined through the fluctuation–dissipation theorem[19]

$$\overleftrightarrow{\epsilon} = \overleftrightarrow{1} + \frac{4\pi}{k_B T V}\langle \vec{M}\vec{M}\rangle, \tag{11}$$

where $\vec{M}$ is the electric-dipole moment, $V$ is the volume, and $T$ is the temperature ($k_B$ is the Boltzmann constant) of the system. Equation (11) is valid in the presence of periodic boundary conditions.[19] We consider a periodically repeated $Ti_2O_4$ unit (see Fig. 1), obtain its 15 independent oscillatory modes, and then calculate $\vec{M}$. Using the law of equipartition for thermal equilibrium among those modes, we compute $\epsilon_{xx}$ (along the $a$ axis) and $\epsilon_{zz}$ (along the $c$ axis) using Eq. (11). Such a calculation yields $\epsilon_{xx} = 91.8$ and $\epsilon_{zz} = 195.9$ at $P = 0$. These results are in close agreement with the experimental values[20,21] of $\epsilon_{xx} = 86$ and $\epsilon_{zz} = 170$ at room temperatures. Note that $\overleftrightarrow{\epsilon}$ is independent of $T$ in the classical harmonic approximation. We can also neglect the electronic polarization effects, since the high-frequency dielectric constants ($\epsilon_{xx}^\infty = 6.8$ and $\epsilon_{zz}^\infty = 8.4$, Ref. 15) are much smaller than their static counterparts ($\epsilon_{xx} = 86$ and $\epsilon_{zz} = 170$). In fact, there is no intra-atom contribution to $\vec{M}$ in the present formulation. We have also investigated the pressure dependence of $\epsilon_{xx}$ and $\epsilon_{zz}$. We find $(\epsilon_{xx}, \epsilon_{zz}) = (90.2, 189.9)$ at $P = 0.2$ GPa and $(\epsilon_{xx}, \epsilon_{zz}) = (88.6, 183.9)$ at $P = 0.4$ GPa. Such a linear decrease in $\epsilon_{xx}$ and $\epsilon_{zz}$ with pressure has been observed experimentally.[21] The calculated slopes, $d\ln\epsilon_{xx}/dP = -0.09$ GPa$^{-1}$ and $d\ln\epsilon_{zz}/dP = -0.15$ GPa$^{-1}$, compare favorably with the experimental results,[21] $d\ln\epsilon_{xx}/dP = -0.05$ GPa$^{-1}$ and $d\ln\epsilon_{zz}/dP = -0.12$ GPa$^{-1}$ at $T = 4$ K.

We have also calculated the surface energies of (110) and (100) surfaces of the rutile structure of $TiO_2$. From the crystalline rutile system, we create a slab (width $\sim 25.0$ Å) with (110) surfaces. The slab is placed in a supercell (19.8 Å $\times$ 19.8 Å $\times$ 33.1 Å), as was done in Ref. 12. Figure 3 shows the atomic positions on the surface, and the axes $u$, $v$, and $w$ along $[\bar{1}10]$, $[001]$, and $[110]$ directions, respectively. The slab contains five Ti layers perpendicular to the $w$ direction. Subsequently the lowest total-energy configuration is obtained with the conjugate-gradient method. Displacement vector $(\Delta u, \Delta v, \Delta w)$ of each atom due to surface relaxation is given in Table III along with the results of the first-principles calculation.[12] Our results for the deviation in the atomic charge from the bulk value, $\Delta q_i = q_i - q_i$(bulk), and the corresponding values from the tight-binding calculation[16] are also listed in Table III. The calculated surface energies
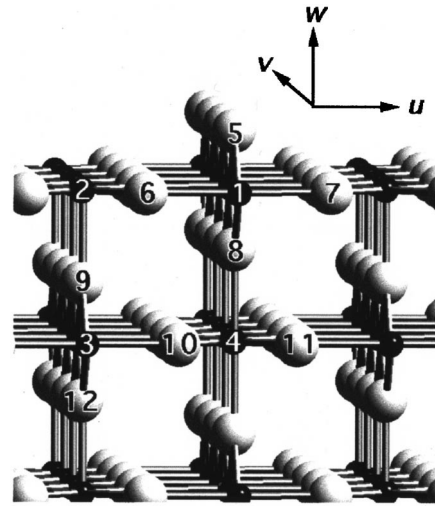


FIG. 3. Atomic configuration of the unrelaxed, stoichiometric (110) surface of rutile. Small and large spheres represent Ti and O atoms, respectively.

are found to be 39 and 41 meV/Å$^2$ while first-principles calculation[12] yield 55 and 70 meV/Å$^2$ for (110) and (100) surfaces, respectively.

To test the transferability of our interaction potential, we have investigated the properties of the anatase[2,4] phase of $TiO_2$. Anatase also has a tetragonal crystal symmetry, but it is a metastable state relative to the rutile structure. We have calculated the ground-state energy of anatase and find it to be larger than that of rutile. The resulting energy difference, 0.09 eV per Ti atom, compares favorably with the heat of formation,[22] 0.068 eV per Ti atom. The lattice constants at zero temperature are determined to be $a = b = 3.85(3.79)$ Å and $c = 8.78(9.51)$ Å where the numbers in the parentheses are the corresponding experimental values;[2] the density has an error of 4%. We have also calculated the dielectric constants along the $a$ and $c$ axes and the values are $\epsilon_{xx} = 38.1$ and $\epsilon_{zz} = 61.6$, respectively. The experimental value of $\epsilon$ for a powder sample of anatase is 48, which is much lower than $\epsilon = 114$ for rutile. Averaging our values for anatase over the

TABLE III. The structural relaxation $(\Delta u, \Delta v, \Delta w)$ and the charge deviation $\Delta q_i$ of the representative atoms in the vicinity of the (110) surface depicted in Fig. 3. The numbers in [ ] for $(\Delta u, \Delta v, \Delta w)$ are cited from the first-principles calculation;[a] those for $\Delta q_i$, from the tight-binding calculations.[b]

| Label | Species | $\Delta u$(Å) | $\Delta v$(Å) | $\Delta w$(Å) | $\Delta q_i$ |
|---|---|---|---|---|---|
| 1 | Ti | 0.0[0.0] | 0.0[0.0] | 0.07[0.13] | −0.02[−0.07] |
| 2 | Ti | 0.0[0.0] | 0.0[0.0] | −0.10[−0.17] | 0.05[−0.01] |
| 3 | Ti | 0.0[0.0] | 0.0[0.0] | −0.10[−0.08] | 0.00[−0.02] |
| 4 | Ti | 0.0[0.0] | 0.0[0.0] | 0.0[0.06] | −0.01[0.01] |
| 5 | O | 0.0[0.0] | 0.0[0.0] | −0.16[−0.06] | 0.09[0.08] |
| 6 | O | −0.04[−0.04] | 0.0[0.0] | −0.09[0.13] | −0.01[0.01] |
| 7 | O | 0.04[0.04] | 0.0[0.0] | −0.09[0.13] | −0.01[0.01] |
| 8 | O | 0.0[0.0] | 0.0[0.0] | −0.07[−0.07] | 0.00[−0.01] |
| 9 | O | 0.0[0.0] | 0.0[0.0] | −0.06[0.02] | ⋯ |
| 10 | O | −0.01[0.05] | 0.0[0.0] | −0.03[−0.03] | ⋯ |
| 11 | O | 0.01[−0.05] | 0.0[0.0] | −0.03[−0.03] | ⋯ |
| 12 | O | 0.0[0.0] | 0.0[0.0] | −0.02[−0.01] | ⋯ |

[a]Reference 23.
[b]Reference 16.

principal directions yields $\epsilon = (2 \times 38.1 + 61.6)/3 \approx 46$. This is in excellent agreement with the experimental value. These results for the anatase phase give us confidence in the transferability of our interaction potential for $TiO_2$.

## IV. DISCUSSION

We have significantly improved the interaction scheme of Streitz and Mintmire by adding a term $\Delta V_{ij}^{TiO}$ [Eq. (7)] to the total potential energy formula [Eq. (1)]. As a result, the calculated anisotropic static dielectric constants, melting temperature, and surface relaxations are in good agreement with experimental results. The term $\Delta V_{ij}^{TiO}$ tends to suppress the imbalance in $q_o$ between neighboring O's. Without this term, the stable crystal structure has a symmetry lower than that of $P4_2/mnm$ (rutile structure).[17] For the (110) surface of rutile, the term $\Delta V_{ij}^{TiO}$ adjusts charges and displacements of atoms on and near the surface. The function $g(R)$ in $\Delta V_{ij}^{TiO}$ [Eq. (7)] increases beyond 0.5 (corresponding to the stoichiometric composition of $TiO_2$) as neighboring O and Ti atoms with equilibrium separations of $\sim\lambda$ approach each other. This behavior of $g(R)$ significantly enhances the degree of ionization of O atoms.

In order to gain insight into how dynamical fluctuations in atomic charges control the dielectric properties of the rutile, we have made a detailed investigation of electric-dipole oscillations in the system. We first note that $\epsilon_{xx}$ is mainly related to the $E_u$ mode[23] in which all Ti atoms on the (001) plane move collectively in a direction that is opposite to the direction of the collective motion of all O atoms. In the case of $\epsilon_{zz}$, the $A_{2u}$ mode,[23] all Ti atoms move collectively along [001] while all O atoms move collectively in the opposite direction. In this context, it is useful to rewrite Eq. (11) as

$$\epsilon_{\mu\mu} = 1 + \sum_l \frac{4\pi e^2 \Sigma_{i,j} q^*_{\mu\mu,i} q^*_{\mu\mu,j}/\sqrt{m_i m_j}}{V \omega_l^2}$$
$$\times \phi_l(i,\mu)\phi_l(j,\mu), \quad (12)$$

where $\phi_l(i,\mu)$ is the $\mu$ component of the eigen vector of the $l$ mode for atom $i$, $\omega_l$ is the frequency of the $l$ mode, and $q^*_{\mu\mu,i}$ is the Born effective charge[23] on atom $i$. The $q^*_{\mu\mu,i}$ is proportional to the polarization of the system induced by a unit displacement of the atomic sublattice in the $\mu$ direction.

The first-principles calculation[23] predicts unusually large $q^*_{\mu\mu,i}$: $q^*_{xx,Ti} = 6.34$, $q^*_{zz,Ti} = 7.54$, $q^*_{xx,O} = -3.17$, and $q^*_{zz,O} = -3.77$. This implies that Ti and O charges exceed 4 and $-2$, respectively. In contrast, our values of $q^*_{\mu\mu,i}$ are close to the bulk equilibrium charges ($q_{Ti} = 2.43$ and $q_O = -1.215$). Thus the elimination of charge optimization does not lead to any appreciable changes in the static dielectric constants; their variations are well within 1%. The large values of $q^*_{\mu\mu,i}$ in the first-principles calculation indicate that the magnitudes of local atomic charges increase significantly

as the Ti–O bond distance increases. Neither $V_{ij}^{es}$ nor $\Delta V_{ij}^{TiO}$ in Eq. (1) gives rise to such an abnormal enhancement of the charge transfer between Ti and O atoms.

Our interatomic potential gives smaller values for the frequencies of the transverse optic modes, 6.18 meV $(A_{2u})$ and 8.94 meV $(E_u)$, than the first-principles calculation[23] [21.8 meV $(A_{2u})$ and 20.4 meV $(E_u)$]. A frequency of $\sim 20$ meV corresponds to a characteristic time of $\sim 200$ fs. Clearly the applicability of the present scheme is limited to time scales larger than $\sim 200$ fs. Therefore, it is desirable to incorporate first-principles results for the bonding between Ti and O atoms in the variable-charge potential scheme. This will allow accurate simulations of short-time phenomena ($<200$ fs) in large-scale $TiO_2$ systems using classical potentials.

An interesting application is the study of properties and processes in nanostructured $TiO_2$. It has been shown[24] that sintering of $TiO_2$ nanopowder during the anatase-to-rutile transformation is an effective way of producing nanophase $TiO_2$ with near-theoretical density. MD simulations of such nanostructured $TiO_2$ are in progress.

[1] SIA Roadmap Coordination Group, *The National Technology Roadmap for Semiconductors* (SIA, Texas, 1997).
[2] Y.-M. Chiang, D. Birnie III, W. D. Kingery, *Physical Ceramics* (Wiley, New York, 1997).
[3] *Nanomaterials Synthesis, Properties, and Application*, edited by A. S. Edelstein and R. C. Cammarata (IOP, London, 1996).
[4] *Concise Encyclopedia of Advanced Ceramic Materials*, edited by R. J. Brook (Pergamon, Cambridge, 1991), pp. 486–488.
[5] C. R. A. Catlow, R. James, W. C. Mackrodt, and R. F. Stewart, Phys. Rev. B **25**, 1006 (1982).
[6] M. Matsui and M. Akaogi, Mol. Simul. **6**, 239 (1991).
[7] K. Fukuda, I. Fujii, and R. Kitoh, Acta Crystallogr., Sect. B: Struct. Sci. **49**, 781 (1993).
[8] F. H. Streitz and J. W. Mintmire, J. Adhes. Sci. Technol. **8**, 853 (1994).
[9] S. Ogata, T. J. Campbell, K. Tsuruta, A. Nakano, R. K. Kalia, P. Vashishta, and C.-K. Loong, Mater. Res. Soc. Symp. Proc. **481**, 625 (1998).
[10] F. H. Streitz and J. W. Mintmire, Phys. Rev. B **50**, 11996 (1994).
[11] A. K. Rappe and W. A. Goddard, J. Phys. Chem. **95**, 3355 (1991).
[12] M. Ramamoorthy, D. Vanderbilt, and R. D. King-Smith, Phys. Rev. B **49**, 16721 (1994).

[13] See, e.g., M. P. Allen and D. J. Tildesley, *Computer Simulation of Liquids* (Oxford, Oxford, 1989).

[14] J. C. Abrahams and J. L. Bernstein, J. Chem. Phys. **55**, 3206 (1971).

[15] J. G. Traylor, H. G. Smith, R. M. Nicklow, and M. K. Wilkson, Phys. Rev. B **3**, 3457 (1971).

[16] P. K. Schelling, N. Yu, and J. W. Halley, Phys. Rev. B **58**, 1279 (1998).

[17] *CRC Handbook of Chemistry and Physics*, 79th ed. (Chemical Rubbe, Boca Raton, 1996).

[18] M. H. Manghnani, J. Geophys. Res. **74**, 4317 (1969).

[19] S. W. de Leeuw, J. W. Perram, and E. R. Smith, Proc. R. Soc. London, Ser. A **373**, 27 (1980).

[20] R. A. Parker, Phys. Rev. **124**, 1719 (1961).

[21] G. A. Samara and P. S. Peercy, Phys. Rev. B **7**, 1131 (1973).

[22] *JANAF Thermodynamic Tables*, 3rd ed., edited by Chase *et al.* (AIP, New York, 1985).

[23] C. Lee, P. Ghosez, and X. Gonze, Phys. Rev. B **50**, 13379 (1994).

[24] K.-N. P. Kumar, K. Keizer, A. J. Burggraaf, T. Okubo, H. Nagamoto, and S. Morooka, Nature (London) **358**, 48 (1992).